Structure of molecular liquids: Hard rod-disk mixtures

David L. Cheung,[1] Lucian Anton,[2,3] Michael P. Allen,[1] and Andrew J. Masters[2]
[1]*Department of Physics and Centre for Scientific Computing, University of Warwick, Coventry, CV4 7AL, United Kingdom*
[2]*School of Chemical Engineering and Analytical Science, University of Manchester, Sackville Street, Manchester, M60 1QD, United Kingdom*
[3]*Institute of Atomic Physics, INFLPR, Lab 22, PO Box MG-36 R76900, Bucharest, Romania*
(Received 31 October 2007; published 31 January 2008)

The structure of hard rod-disk mixtures is studied using Monte Carlo simulations and integral equation theory, for a range of densities in the isotropic phase. By extension of methods used in single component fluids, the pair correlation functions of the molecules are calculated and comparisons between simulation and integral equation theory, using a number of different closure relations, are made. Comparison is also made for thermodynamic data and phase behavior.

DOI: 10.1103/PhysRevE.77.011202 PACS number(s): 61.20.Gy, 61.20.Ja, 05.20.Jj

I. INTRODUCTION

Fluids composed of mixtures of nonspherical molecules show a rich phase behavior which poses challenging theoretical and computational questions. Their microscopic structure has been investigated in the past decades with a variety of tools: Monte Carlo (MC) simulation [1–3] and Onsager theory and its improved versions [4–6], leading to the latest version of density functional theory [7,8]. Mixtures of rod- and disk-shaped particles have attracted special interest: They have been shown to form a range of liquid crystal phases, including biaxial phases [1].

As for single component fluids, the microscopic structure of a fluid mixture is important in determining, e.g., thermodynamics or phase behavior [9,10]. In this paper, we compute the microscopic properties of rod-disk molecular mixtures using MC simulations and integral equation theory (IET). A key component of the theory is the closure relation, most generally formulated by defining a function called the bridge function. We continue the exploration of the bridge function for fluids made of nonspherical molecules that we have started in our previous work [11,12]. The system studied here is a binary mixture of prolate and oblate axially symmetric spheroids of equal volume and characterized by the major diameters A_p, B_o and minor diameters B_p, A_o, respectively, with aspect ratios (elongations) $e_p=A_p/B_p=3$, $e_o=A_o/B_o=1/3$. MC simulations are used to compute the two-particle distribution function; from the Ornstein-Zernike (OZ) equation we can obtain the direct correlation function and the bridge function. The MC results are compared to IET in two versions: The hypernetted chain (HNC) approximation and an improved closure that uses the so-called modified Verlet bridge function (MV).

This paper is organized as follows. Section II presents the general formalism in the case of a binary mixture for the spherical harmonic expansion of the distribution function of interest, the OZ equation, and IET. Section III presents the details of the MC calculation; the numerical results are discussed in Sec. IV. The conclusions are presented in Sec. V.

II. GENERAL FORMALISM

A. Correlation function and their angular expansion

In order to establish notation we present briefly the mixture correlation functions. The formal relations between the correlation functions described in Ref. [11] can be used directly in this paper if one adds a species label to the position and the orientation coordinates of each molecule. The pair functions of interest depend on the intermolecular vector $\boldsymbol{r}_{12}$, the molecular orientations $\boldsymbol{u}_1$ and $\boldsymbol{u}_2$, and the particle species α, β (prolate or oblate) of the given molecules. In order to facilitate their calculation from simulation and IET, the angular variation of these functions is expanded in basis sets of spherical harmonics $Y_{\ell m}(\boldsymbol{u})$. There are two useful choices for this expansion [9,13]. The first is the laboratory frame in which an arbitrary pair function $F_{\alpha\beta}(1,2)\equiv F_{\alpha\beta}(\boldsymbol{u}_1,\boldsymbol{u}_2,\boldsymbol{r}_{12})$ is expanded as follows:

$$F_{\alpha\beta}(1,2)=\sum_{\ell_1\ell_2\ell} F_{\alpha\beta}^{\ell_1\ell_2\ell}(r_{12})\Phi_{\ell_1\ell_2\ell}(\boldsymbol{u}_1,\boldsymbol{u}_2,\hat{\boldsymbol{r}}_{12}). \quad (1)$$

Here $r_{12}=|\boldsymbol{r}_{12}|$ is the center-center separation and $\hat{\boldsymbol{r}}_{12}=\boldsymbol{r}_{12}/|\boldsymbol{r}_{12}|$ is the unit vector along $\boldsymbol{r}_{12}$. The expansion functions $\Phi_{\ell_1\ell_2\ell}$ are rotational invariants defined by

$$\Phi_{\ell_1\ell_2\ell}(\boldsymbol{u}_1,\boldsymbol{u}_2,\hat{\boldsymbol{r}}_{12})=4\pi\sum_{m_1m_2m}\begin{pmatrix}\ell_1 & \ell_2 & \ell\\ m_1 & m_2 & m\end{pmatrix}\times Y_{\ell_1m_1}(\boldsymbol{u}_1)Y_{\ell_2m_2}(\boldsymbol{u}_2)C_{\ell m}(\hat{\boldsymbol{r}}_{12}), \quad (2)$$

where $C_{\ell m}(\hat{\boldsymbol{r}}_{12})=\sqrt{4\pi/(2\ell+1)}Y_{\ell m}(\hat{\boldsymbol{r}}_{12})$ and the $\begin{pmatrix}\ell_1 & \ell_2 & \ell\\ m_1 & m_2 & m\end{pmatrix}$ are the standard $3j$ coefficients.

The alternative choice is the molecular frame, where the intermolecular vector is taken to be parallel to the z axis. In this frame the expansion reads

$$F_{\alpha\beta}(1,2)=4\pi\sum_{\ell_1\ell_2\chi} F_{\ell_1\ell_2\chi}^{\alpha\beta}(r_{12})Y_{\ell_1\chi}(\boldsymbol{u}_1)Y_{\ell_2\bar{\chi}}(\boldsymbol{u}_2), \quad (3)$$

where $\bar{\chi}=-\chi$. The expansion coefficients may be transformed between frames via the so-called "chi" transform and its inverse

$$F^{\alpha\beta}_{\ell_1\ell_2\chi}(r) = \sum_{\ell} \begin{pmatrix} \ell_1 & \ell_2 & \ell \\ \chi & \bar{\chi} & 0 \end{pmatrix} F^{\ell_1\ell_2\ell}_{\alpha\beta}(r), \tag{4a}$$

$$F^{\ell_1\ell_2\ell}_{\alpha\beta}(r) = (2\ell+1)\sum_{\chi} \begin{pmatrix} \ell_1 & \ell_2 & \ell \\ \chi & \bar{\chi} & 0 \end{pmatrix} F^{\alpha\beta}_{\ell_1\ell_2\chi}(r). \tag{4b}$$

It is often more convenient to work in reciprocal space. Both the laboratory and molecular frame expansions may still be used for the Fourier-transformed pair function $\tilde{F}_{\alpha\beta}(1,2) \equiv \tilde{F}_{\alpha\beta}(\boldsymbol{u}_1,\boldsymbol{u}_2,\boldsymbol{k})$

$$\tilde{F}_{\alpha\beta}(1,2) = 4\pi \sum_{\ell_1\ell_2\ell} \tilde{F}^{\ell_1\ell_2\ell}_{\alpha\beta}(k)\Phi_{\ell_1\ell_2\ell}(\boldsymbol{u}_1,\boldsymbol{u}_2,\hat{\boldsymbol{k}}), \tag{5a}$$

$$\tilde{F}_{\alpha\beta}(1,2) = 4\pi \sum_{\ell_1\ell_2\chi} \tilde{F}^{\alpha\beta}_{\ell_1\ell_2\chi}(k)Y_{\ell_1\chi}(\boldsymbol{u}_1)Y_{\ell_2\bar{\chi}}(\boldsymbol{u}_2). \tag{5b}$$

The corresponding expansion coefficients are linked again by the chi-transform. The molecular frame coefficients in real and reciprocal space are linked by the Hankel transform

$$\tilde{F}^{\ell_1\ell_2\ell}_{\alpha\beta}(k) = 4\pi i^{\ell} \int dr\, r^2 F^{\ell_1\ell_2\ell}_{\alpha\beta}(r) j_{\ell}(kr), \tag{6a}$$

$$F^{\ell_1\ell_2\ell}_{\alpha\beta}(r) = (2\pi^2)^{-1}(-i)^{\ell} \int dr\, k^2 \tilde{F}^{\ell_1\ell_2\ell}_{\alpha\beta}(k) j_{\ell}(kr), \tag{6b}$$

where $j_\ell(x)$ is a spherical Bessel function. The $\tilde{F}^{\alpha\beta}_{\ell_1\ell_2\chi}(k)$ are found from the $\tilde{F}^{\ell_1\ell_2\ell}_{\alpha\beta}(k)$ using the chi transform. As the pair functions are invariant under exchange of molecules the expansion coefficients satisfy the conditions $F^{\ell_1\ell_2\ell}_{\alpha\beta}(r) = F^{\ell_2\ell_1\ell}_{\beta\alpha}(r)$ and $F^{\alpha\beta}_{\ell_1\ell_2\chi}(r) = F^{\beta\alpha}_{\ell_2\ell_1\chi}(r)$.

B. Ornstein-Zernike equation and integral equation theory

On a two-particle level, the structure of a multicomponent fluid may be described by the set of total correlation functions $h_{\alpha\beta}(1,2)$, or the direct correlation functions $c_{\alpha\beta}(1,2)$, where α,β run over all components. These functions are linked via the Ornstein-Zernike equation, which for a mixture of uniaxial particles reads

$$h_{\alpha\beta}(1,2) = c_{\alpha\beta}(1,2) + \frac{\rho}{4\pi}\sum_{\gamma} \int d3\; c_{\alpha\gamma}(1,3)x_\gamma h_{\gamma\beta}(3,2), \tag{7}$$

where ρ is the number density and x_γ is the number fraction of component γ. The integration is over the position and orientation of molecule 3.

For a self-consistent calculation, the OZ equation must be supplemented with a closure relationship between the functions $h_{\alpha\beta}$ and $c_{\alpha\beta}$, which can be obtained by straightforward generalization of the one-component case [11]. The exact closure reads

$$c_{\alpha\beta}(1,2) = [f_{\alpha\beta}(1,2)+1]\exp[\eta_{\alpha\beta}(1,2)+b_{\alpha\beta}(1,2)] - \eta_{\alpha\beta}(1,2) - 1, \tag{8}$$

where

$$f_{\alpha\beta}(1,2) = \exp[-\beta V_{\alpha\beta}(1,2)] - 1 = \begin{cases} -1, & \text{if the two molecules overlap,} \\ 0, & \text{otherwise} \end{cases}$$

is the Mayer function and $\eta_{\alpha\beta}(1,2) = h_{\alpha\beta}(1,2) - c_{\alpha\beta}(1,2)$. This equation serves to define the set of bridge functions $b_{\alpha\beta}(1,2)$; approximate theories usually propose a relationship between these functions and $\eta_{\alpha\beta}(1,2)$.

In this paper, we study the HNC closure, $b_{\alpha\beta}(1,2)=0$, and a modified Verlet (MV) bridge function [14,15] defined by

$$b_{\alpha\beta}(1,2) = -\frac{\frac{1}{2}\eta^2_{\alpha\beta}(1,2)}{1+\nu_{\alpha\beta}\eta_{\alpha\beta}(1,2)}. \tag{9}$$

The coefficients $\nu_{\alpha\beta}$ depend on the total number density ρ and the component number fractions x_α. In the present case we specialize to two components, defined by x_p (prolate) and $x_o = 1 - x_p$ (oblate). The functional form of the $\nu_{\alpha\beta}$ is determined by a combination of heuristical arguments aimed to reduce the thermodynamic inconsistency of the equation of state. In our case we follow Ref. [16] and use the effective spheroid diameters d_{pp} and d_{oo}, defined as the diameter of the sphere equal in volume to a given spheroid; thus $d^3_{pp} = A_p B^2_p$, etc. The interspecies effective diameter is defined as $d_{po} = d_{op} = (d_{pp}+d_{oo})/2$. The full expressions are of the form

$$\nu_{\alpha\beta} = a_{\alpha\beta}e^{-2\xi} + 0.8 - 0.45\xi, \tag{10}$$

where $\xi = (\pi/6)\rho(x_p d^3_{pp} + x_o d^3_{oo})$ is the packing fraction and the $a_{\alpha\beta}$ coefficients depend upon the number fractions and diameters. In fact, in this work, we specialize to spheroids of equal volume, so all the diameters are equal $d_{\alpha\beta}=d$, and the expressions simplify to

$$a_{\alpha\beta} = \frac{17}{120\xi}. \tag{11}$$

The coefficients $b^{mnl}_{\alpha\beta}(r)$ of the rotational invariant expansion of the bridge function are computed from Eq. (9), where the product expansion of the rotational invariants is used [17]. Starting from the equivalent form

$$[1+\nu_{\alpha\beta}\eta_{\alpha\beta}(1,2)]b_{\alpha\beta}(1,2) = -\tfrac{1}{2}\eta^2_{\alpha\beta}(1,2),$$

and using the rotational invariant expansion, a linear system is obtained for the coefficients $b^{mnl}_{\alpha\beta}(r)$ for each value of the discretized r.

The numerical solution of the coupled set of nonlinear equations resulting from the discretization of the OZ and HNC or MV equation is obtained using the iterative Newton solver developed in Ref. [18].

III. SIMULATION

The total correlation function may be determined directly from simulation through the pair distribution function $g_{\alpha\beta}(1,2)$. The spherical harmonic coefficients are determined as usual from [19]

$$g^{\alpha\beta}_{mn\chi}(r) = 4\pi g^{\alpha\beta}_{000}(r)\langle Y^*_{m\chi}(\boldsymbol{u}_1)Y^*_{n\bar{\chi}}(\boldsymbol{u}_2)\rangle_r, \tag{12}$$

where $g^{\alpha\beta}_{000}(r)$ is the pair distribution function of the particle centers and the angled brackets denote an average over all

molecules in the shell $[r, r+\delta r]$. These coefficients are defined in the molecular frame described in Sec. II A [9]. From Eq. (12) it follows that $h^{\alpha\beta}_{mn\chi}(r) = g^{\alpha\beta}_{mn\chi}(r) - \delta_{m0}\delta_{n0}\delta_{\chi 0}$.

Since the OZ equation has the form of a convolution, it is most conveniently solved in reciprocal space. Using the molecular frame expansion Eq. (5b) in Eq. (7) we have

$$\tilde{h}^{\alpha\beta}_{\ell_1\ell_2\chi}(k) - \tilde{c}^{\alpha\beta}_{\ell_1\ell_2\chi}(k) = (-1)^{\chi}\rho \sum_{\ell_3,\gamma} \tilde{c}^{\alpha\gamma}_{\ell_1\ell_3\chi}(k) x_\gamma \tilde{h}^{\gamma\beta}_{\ell_3\ell_2\chi}(k). \tag{13}$$

This set of linear equations may then be solved to give the $\tilde{c}^{\alpha\beta}_{\ell_1\ell_2\chi}(k)$ from which the real-space functions $c_{\alpha\beta}(1,2)$ may be determined.

The cavity function, defined by the relation $y_{\alpha\beta}(1,2)[1+f_{\alpha\beta}(1,2)] = g_{\alpha\beta}(1,2)$, is determined by directly simulating a system containing two noninteracting cavity particles [20]. In order to effectively sample $y_{\alpha\beta}(1,2)$ across a range of separations, generalized umbrella sampling is employed, with a bias function found iteratively using the Wang-Landau algorithm [21,22]. Full details of this method may be found in Ref. [11].

The spherical harmonic coefficients of the bridge function $b_{\alpha\beta}(1,2)$ may be determined by inverting the exact closure relation [Eq. (8)], which may be written as

$$y_{\alpha\beta}(1,2) = \exp[h_{\alpha\beta}(1,2) - c_{\alpha\beta}(1,2) + b_{\alpha\beta}(1,2)]. \tag{14}$$

The presence of the exponential on the right-hand side of Eq. (14) is troublesome for the spherical harmonic expansions, but it may be easily circumvented [11,17]. Taking the logarithm and differentiating Eq. (14) with respect to r gives

$$\frac{\partial y_{\alpha\beta}(1,2)}{\partial r} = y_{\alpha\beta}(1,2)\left[\frac{\partial h_{\alpha\beta}(1,2)}{\partial r} - \frac{\partial c_{\alpha\beta}(1,2)}{\partial r} + \frac{\partial b_{\alpha\beta}(1,2)}{\partial r}\right]. \tag{15}$$

Inserting the spherical harmonic expansions of the pair functions and integrating over angles gives [9]

$$\frac{dy^{\alpha\beta}_{mn\chi}(r)}{dr} = 4\pi \sum_{\substack{m'n'\chi' \\ m''n''\chi''}} \Gamma^{mm'm''}_{\chi\chi'\chi''}\Gamma^{nn'n''}_{\bar{\chi}\bar{\chi}'\bar{\chi}''} y^{\alpha\beta}_{m''n''\chi''}(r)\frac{d}{dr}[h^{\alpha\beta}_{m'n'\chi'}(r) - c^{\alpha\beta}_{m'n'\chi'}(r) + b^{\alpha\beta}_{m'n'\chi'}(r)], \tag{16}$$

where

$$\Gamma^{mm'm''}_{\chi\chi'\chi''} = \int d\boldsymbol{u}\; Y^*_{m\chi}(\boldsymbol{u}) Y_{m'\chi'}(\boldsymbol{u}) Y_{m''\chi''}(\boldsymbol{u}) = \sqrt{\frac{(2m'+1)(2m''+1)}{4\pi(2m+1)}} \times C(m'',m',m;0,0,0)C(m'',m',m;\chi'',\chi',\chi), \tag{17}$$

and where $C(m'',m',m;\chi'',\chi'\chi)$ are Clebsch-Gordan coefficients. Equation (15) can be solved using standard numerical methods [23] for the derivatives $db^{\alpha\beta}_{mn\chi}(r)/dr$, and these are integrated numerically to give the bridge function components $b^{\alpha\beta}_{mn\chi}(r)$.

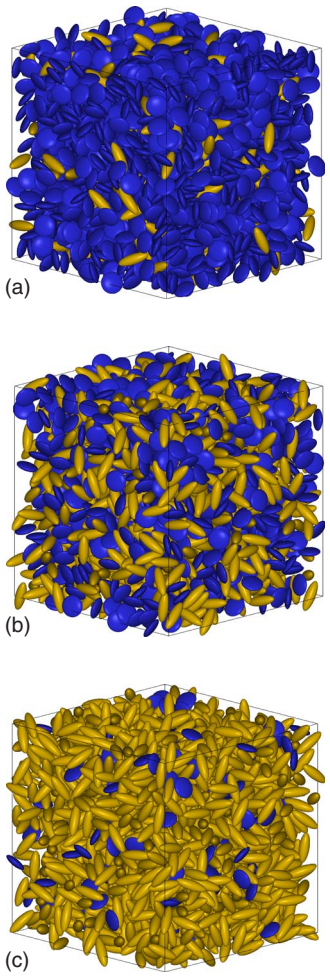

FIG. 1. (Color online) Simulation snapshots for rod-disk mixtures with $x_p=0.10$ (top), $x_p=0.50$ (middle), and $x_p=0.90$ (bottom) at $\rho^*=0.50$. (Online: rods yellow, disks blue). Snapshots generated using the QMGA package [24].

Systems consisting of 2000 molecules were simulated in the isotropic phase using constant-*NVT* MC simulations. The systems consisted of mixtures of ellipsoids with elongations $e_p=A_p/B_p=3$ and $e_o=A_o/B_o=1/3$. The ellipsoid axes were selected to give equal molecular volumes for both components: Taking $A_p=e_p$ and $B_p=1$ gives $A_o=e_o^{1/3}$ and $B_o=e_o^{-2/3}$. Simulations were performed at densities $\rho B_p^3=0.047$, 0.094, 0.141, 0.188, 0.235, 0.283, and 0.306. These densities are equivalent to reduced densities (relative to the close packed density for a single component system) of $\rho^*=\rho/\rho_{\mathrm{cp}}=0.10$, 0.20, 0.30, 0.40, 0.50, 0.60, and 0.65. Systems with rod fractions $x_p=1-x_o=1.00$, 0.90, 0.75, 0.60, 0.50, 0.40, 0.25, 0.10, and 0.00 were studied. Example simulation snapshots are shown in Fig. 1. $h_{\alpha\beta}(1,2)$ components were determined in the usual manner, statistics for which were gathered over four million MC sweeps (one attempted translation and rotation per particle), split into four subruns. The $c_{\alpha\beta}(1,2)$ components were then determined from Eq. (13). Systems consisting of 500 molecules were used for the calculation of the

TABLE I. Window intervals used in calculation of cavity function.

α, β	Window intervals (r/B_p)
p, p	[0.03, 0.50], [0.20, 1.20], [1.00, 2.00], [1.80, 2.80], [2.60, 3.60]
p, o	[0.03, 0.50], [0.20, 1.20], [1.00, 2.00], [1.80, 2.80]
o, o	[0.03, 0.50], [0.20, 1.20], [1.00, 2.00], [1.80, 2.30]

cavity function. The r separation between the cavity particles was split into overlapping windows, which are listed in Table I [note that, at separations greater than the interaction range, $y_{\alpha\beta}(1,2) \rightarrow 1+h_{\alpha\beta}(1,2)$]. The weight function for each window was determined using Wang-Landau sampling over two million MC sweeps. Once the final weight function was determined, $y(1,2)$ data were gathered over a total of 2×10^7 MC sweeps, divided into four subruns.

IV. RESULTS

A. Direct and total correlation functions

Shown in Figs. 2 and 3 are selected components of the direct correlation function (DCF) $c_{\alpha\beta}(1,2)$ for the equimolar $(x_p=0.5)$ mixture. At low density $(\rho^*=0.20)$ there is good agreement between the components found from simulation and those calculated using IET using both HNC and MV closures. At higher density $(\rho^*=0.50)$ marked discrepancies appear between the DCF components calculated using HNC closure and those found from simulation. This is most noticeable in the isotropic $c_{000}^{\alpha\beta}$ components. In contrast, the DCF components calculated using the MV closure remain in good agreement with simulation.

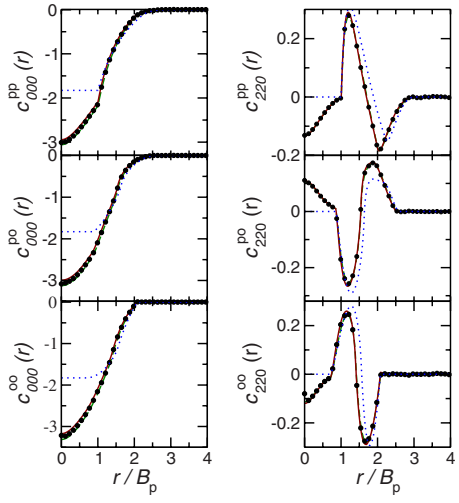

FIG. 2. (Color online) Components of the direct correlation function (evaluated in the molecular frame) for the $x_p=0.50$ mixture at density $\rho^*=0.20$. Components found from MC simulations are denoted by circles, those from IET using the HNC closure denoted by the solid line, IET using the MV closure denoted by dashed line, and the Parsons-Lee DCF is denoted by the dotted line. The statistical error in the MC results is smaller than the symbol size. Note that the HNC and MV results for the $c_{220}^{\alpha\beta}(r)$ are indistinguishable on the above scale.

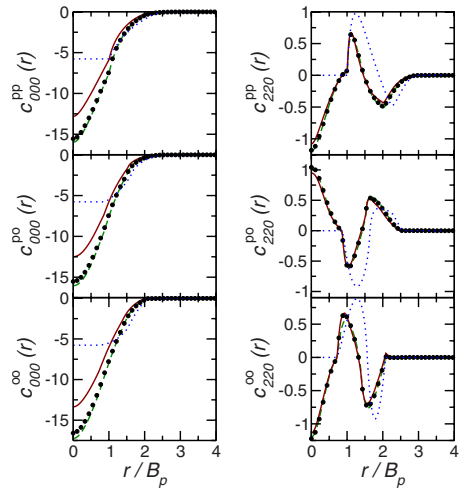

FIG. 3. (Color online) Components of the direct correlation function (evaluated in the molecular frame) for the $x_p=0.50$ mixture at density $\rho^*=0.50$. Symbols as in Fig. 2. The statistical error in the MC results is smaller than the symbol size.

DCF components for the asymmetric mixture with $x_p=0.90$ at $\rho^*=0.50$ are shown in Fig. 4. It is noticeable that there is very little difference between the DCF components, both from simulation and IET, for this mixture and the symmetric case. In fact, this holds true for all mixture compositions. As for the symmetric mixture, the DCF components calculated using the MV closure are in better agreement with simulation than those calculated using the HNC closure.

Also shown in Figs. 2–4 are components of the Parsons-Lee (PL) DCF [25–27], which is given by

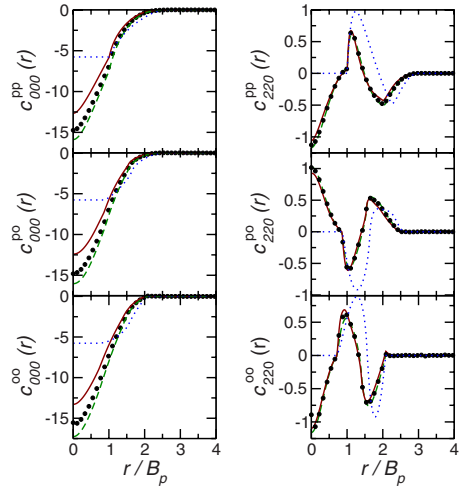

FIG. 4. (Color online) Components of the direct correlation function (evaluated in the molecular frame) for the $x_p=0.90$ mixture at density $\rho^*=0.50$. Symbols as in Fig. 2. The statistical error in the MC results is smaller than the symbol size.

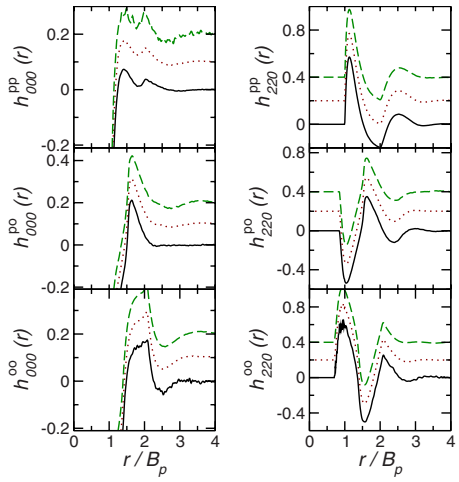

FIG. 5. (Color online) Components of the total correlation function (evaluated in the molecular frame) found from MC simulations at $\rho^*=0.50$. The solid line denotes the $x_p=0.90$ mixture, dotted line $x_p=0.50$, and dashed line $x_p=0.10$. Successive curves are offset by 0.1 $[h^{\alpha\beta}_{000}(r)]$ or 0.2 $[h^{\alpha\beta}_{220}(r)]$ units for clarity.

$$c^{\mathrm{PL}}_{\alpha\beta}(1,2)=\frac{1-\eta/4}{(1-\eta)^4}f_{\alpha\beta}(1,2), \tag{18}$$

where η is the packing fraction. In the partial overlap region the 000 component is in reasonable agreement with the MC and IET data. At low density there is also fair agreement with the 220 component in this region. However, at higher density the comparison is much poorer, in agreement with previous comparisons for the single component fluid [28]. In the core region the PL DCF fails completely [as $f_{\alpha\beta}(1,2)=-1$ here]. In all cases the DCF components calculated using IET are in better agreement with MC results than those from PL theory.

The effect of changing mixture composition may be seen in $h_{\alpha\beta}(1,2)$. Shown in Fig. 5 are selected $h^{\alpha\beta}_{mn\chi}(r)$ components, calculated from simulation (components calculated using the IET give similar results). The change in $h_{\alpha\beta}(1,2)$ with mixture composition is most noticeable in the region $2.5\leq r/B_p\leq 3.5$.

B. Bridge function

Shown in Figs. 6 and 7 are selected bridge function components for the $x_p=0.5$ mixture, calculated from MC simulations and IET using the Verlet bridge closure [for the HNC closure $b_{\alpha\beta}(1,2)=0$]. At low densities ($\rho^*=0.20$) these are in good agreement with each other, with some discrepancies in the region $r\to 0$. For higher densities ($\rho^*=0.50$) the difference between the simulation and IET-MV bridges is more apparent. This discrepancy is most noticeable in the "like" components $b^{pp}_{mn\chi}(r)$ and $b^{oo}_{mn\chi}(r)$, which are overestimated in the MV results. It should be noted that the bridge function components calculated using MV closure are however, in much better agreement with simulation than those calculated using the Percus-Yevick closure or from a low order virial expansion [11].

Shown in Fig. 8 are components of the bridge function for the $x_p=0.10$ and $x_p=0.90$ mixtures at $\rho^*=0.50$. For these

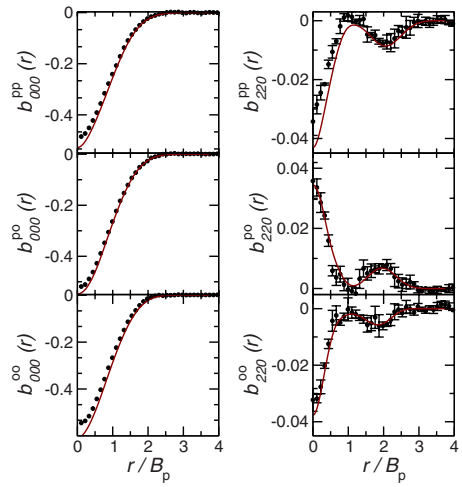

FIG. 6. (Color online) Components of the bridge function (evaluated in the molecular frame) for the $x_p=0.50$ mixture at $\rho^*=0.20$. Simulation data denoted by circles; IET-MV data shown by solid line. For the $b_{000}(r)$ components (left) the statistical error in the MC results is smaller than the symbol size.

mixture compositions there is little difference between the simulation bridge function components. However, the magnitude of the bridge function components for these compositions are smaller than those for the symmetric mixture. By contrast the bridge functions calculated using the MV closure are of larger magnitude than for the symmetric case. There is also a larger difference between the components for the $x_p=0.10$ and $x_p=0.90$ mixtures than in the MC results.

More insight into the bridge function may be gained from the so-called Duh-Haymet plots [29], in which the $b_{\alpha\beta}(1,2)$ are plotted as functions of $\eta_{\alpha\beta}(1,2)$. Shown in Fig. 9 are DH plots for the $x_p=0.10$, $x_p=0.50$, and $x_p=0.90$ mixtures at $\rho^*=0.50$. The data points in Fig. 9 correspond to values of $b_{\alpha\beta}(1,2)$ and $\eta_{\alpha\beta}(1,2)$ for fixed orientations given defined

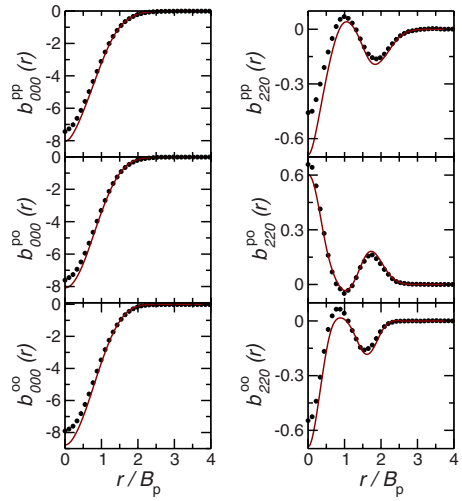

FIG. 7. (Color online) Components of the bridge function (evaluated in the molecular frame) for the $x_p=0.50$ mixture at $\rho^*=0.50$. Symbols as in Fig. 6. The statistical error in the MC results is smaller than the symbol size.

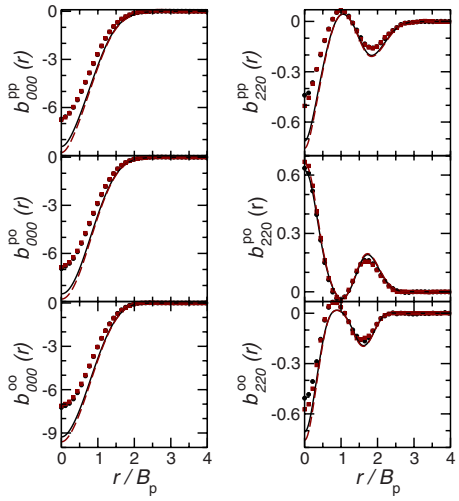

FIG. 8. (Color online) Components of the bridge function (evaluated in the molecular frame) for the $x_p=0.90$ and $x_p=0.10$ mixtures at $\rho^*=0.50$ calculated from MC simulation and IET with MV closure. Data for $x_p=0.90$ mixture shown by circles (MC) and solid line (MV), and $x_p=0.10$ squares (MC) and dashed line (MV). The statistical error in the MC results is smaller than the symbol size.

Table II. Also shown are the results for the one-component $e=3$ and $e=1/3$ fluids [12]. While there is a degree of scatter in the MC results, bridge functions for different orientations and mixture compositions fall approximately on the same curve. In addition, the plots of $b_{\alpha\beta}(r)$ fall on similar curves for the different α,β. This is consistent with the behavior seen for single component fluids of spheroids where there is good agreement between bridge functions for spheroids of elongation e and $1/e$ [12]. Comparison with the MV bridge function shows that this overestimates the magnitude of $b_{\alpha\beta}(1,2)$.

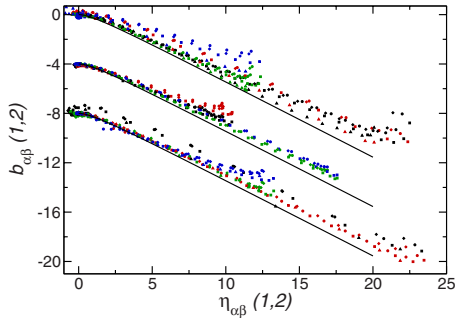

FIG. 9. (Color online) Duh-Haymet plots of bridge functions for fixed orientations for mixtures with $x_p=0.10$ (circles), $x_p=0.50$ (squares), and $x_p=0.90$ (diamonds) at $\rho^*=0.50$. The triangles show the bridge function for the single component $e=3$ and $e=1/3$ fluids and the solid lines denote the MV bridge function. Orientations are defined in Table II: e, s, t, x (color online: black, red, green, blue, respectively). Duh-Haymet plots for *po* and *oo* are shifted down by four and eight units, respectively, for clarity.

TABLE II. Orientations of molecules (with respect to center-center vector $\boldsymbol{r}$) used in Duh-Haymet plots (Fig. 9). The relative orientation angles are defined by $\cos\theta_1=\boldsymbol{u}_1\cdot\hat{\boldsymbol{r}}$, $\cos\theta_2=\boldsymbol{u}_2\cdot\hat{\boldsymbol{r}}$, and $\cos\phi=\hat{\boldsymbol{p}}_1\cdot\hat{\boldsymbol{p}}_2$, where $\hat{\boldsymbol{p}}_i$ is the unit vector in the direction $\boldsymbol{p}_i=\boldsymbol{u}_i\times\hat{\boldsymbol{r}}$.

Orientation	e	s	t	x
ϕ (deg)	0	0	0	90
θ_1 (deg)	0	90	0	90
θ_2 (deg)	0	90	90	90

C. Equation of state and stability

Shown in Fig. 10 is the equation of state data for the $x_p=0.50$ and $x_p=0.90$ mixtures, found from MC simulations and IET theory. This is an important test: The equation of state found using a thermodynamically self-consistent closure would be the same when found using either the virial (V) or compressibility (C) routes [10].

At low densities, there is good agreement between the different closures and the MC data. There is also only a small difference between V and C equations of state. On increasing density, a large gap between the V and C equations of state appears for the HNC closure. The MV closure is seen to significantly reduce the gap between these. The different equations of state for both closures bracket the MC equation of state. The relative magnitudes of the V and C equations of state change for the two closures. We note also that the variation of the prolate fraction induces a slight shift in the equation of state curves, but with a similar thermodynamic inconsistency gap.

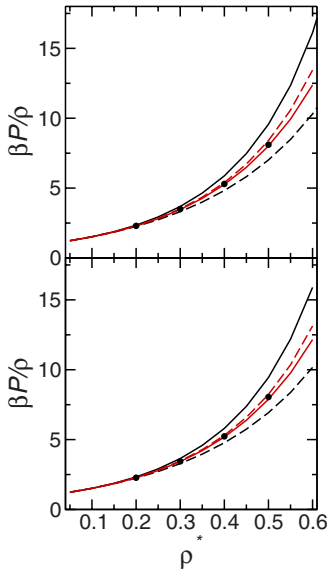

FIG. 10. (Color online) Equation of state $\beta P/\rho$ where P is the pressure, $\beta=1/k_BT$, and ρ is the density, plotted against reduced density ρ^*, for $x_p=0.50$ (top) and $x_p=0.90$ (bottom) mixtures. MC data shown by circles, HNC is shown in black and MV by gray (online red), with the virial and compressibility equations of state shown by the solid and dashed lines. The statistical error in the MC results is smaller than the symbol size.

From density functional theory, the stability of the isotropic phase with respect to the nematic phase may be determined from the direct correlation function in the isotropic phase [30]. For a one-component system, the isotropic phase is stable when the Kerr coefficient

$$K = 1 - \frac{\rho}{\sqrt{5}}\tilde{c}^{220} > 0, \tag{19}$$

where $\tilde{c}^{220} \equiv \tilde{c}^{220}(k=0)$ is the Fourier transform of the relevant angular component of the direct correlation function evaluated in the laboratory frame, at zero wave number. For a two-component mixture K is given by the determinant of the stability matrix

$$K = \begin{vmatrix} 1 - \frac{\rho_p}{\sqrt{5}}\tilde{c}^{220}_{pp} & \sqrt{\frac{\rho_p\rho_o}{5}}\tilde{c}^{220}_{po} \\ \sqrt{\frac{\rho_p\rho_o}{5}}\tilde{c}^{220}_{po} & 1 - \frac{\rho_o}{\sqrt{5}}\tilde{c}^{220}_{oo} \end{vmatrix}, \tag{20}$$

where again the Fourier transforms are evaluated at $k=0$.

Figure 11 shows that, in contrast to the equation of state, the HNC solution provides a better description of the Kerr coefficient than the MV closure. Both the MC and IET Kerr coefficients vary monotonically with x_p.

V. CONCLUSIONS

Using MC simulations and IET, with two different closure relations, the correlation functions and thermodynamics are studied for a mixture of rod- and disk-shaped molecules, at a range of densities and mixture compositions in the isotropic phase. From MC simulation, the direct correlation function is found to be insensitive to changing the mixture composition, while the total correlation function shows some systematic variation with changing x_p. At low densities, good agreement is found between MC and IET using both HNC and MV closures. For higher densities, significant discrepancies appear between MC and HNC results, whereas MV results remain in good agreement. This remains true when the mixture composition changes. Bridge function components found in MC simulations agree well with those calculated from IET using the MV closure, particularly at low densities.

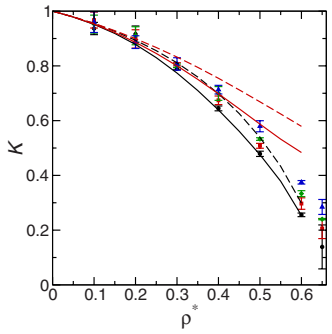

FIG. 11. (Color online) Determinant of the stability matrix (Kerr coefficient) against density. The symbols denote MC results for $x_p=0.10$ (circles, online black), $x_p=0.40$ (squares, online red), $x_p=0.60$ (diamonds, online green), and $x_p=0.90$ (triangles, online blue). Black lines denote HNC results for $x_p=0.10$ (solid) and $x_p=0.90$ (dashed) and the gray (red online) lines denote MV results for $x_p=0.10$ (solid line) and $x_p=0.90$ (dashed line). Data for intermediate x_p fall between these lines, varying monotonically with respect to x_p.

Comparison of thermodynamic properties also shows that the MV closure is superior to the HNC closure. This is most noticeable in the equation of state, where the inconsistency between the compressibility and virial equations of state is significantly smaller using the MV closure than using the HNC closure. However, in common with the single-component system [12,15], the stability of the isotropic phase with respect to the nematic is poorly described by the MV closure.

ACKNOWLEDGMENTS

This work was supported by EPSRC Grants No. GR/S77240 and No. GR/S77103. Computational resources were provided by the Centre for Scientific Computing, University of Warwick and Manchester Computing, University of Manchester.

[1] P. J. Camp and M. P. Allen, Physica A **229**, 410 (1996).
[2] P. J. Camp, M. P. Allen, P. G. Bolhuis, and D. Frenkel, J. Chem. Phys. **106**, 9270 (1997).
[3] X. Zhou, H. Chen, and M. Iwamoto, J. Chem. Phys. **120**, 1832 (2004).
[4] A. Stroobants and H. N. W. Lekkerkerker, J. Phys. Chem. **88**, 3669 (1984).
[5] H. N. W. Lekkerkerker, P. Coulon, R. Van Der Haegen, and R. de Bliek, J. Chem. Phys. **80**, 3427 (1984).
[6] K. R. Purdy, S. Varga, A. Galindo, G. Jackson, and S. Fraden, Phys. Rev. Lett. **94**, 057801 (2005).
[7] A. Chamoux and A. Perera, J. Chem. Phys. **104**, 1493 (1996).
[8] M. Moradi and R. Khordad, J. Chem. Phys. **125**, 214504 (2006).
[9] C. G. Gray and K. E. Gubbins, *Theory of Molecular Fluids. 1. Fundamentals* (Clarendon Press, Oxford, 1984).
[10] J.-P. Hansen and I. R. McDonald, *Theory of Simple Liquids*, 2nd ed. (Academic Press, London, 1986).
[11] D. L. Cheung, L. Anton, M. P. Allen, and A. J. Masters, Phys. Rev. E **73**, 061204 (2006).
[12] D. L. Cheung, L. Anton, M. P. Allen, and A. J. Masters, Phys. Rev. E **76**, 041201 (2007).
[13] L. Blum and A. J. Torruella, J. Chem. Phys. **56**, 303 (1972).
[14] S. Labík, A. Malijevský, and W. R. Smith, Mol. Phys. **73**, 87 (1991).
[15] R. Pospísil, A. Malijevský, and W. R. Smith, Mol. Phys. **79**, 1011 (1993).
[16] D. Henderson, A. Malijevský, S. Labík, and K. Y. Chan, Mol. Phys. **87**, 273 (1996).
[17] P. H. Fries and G. N. Patey, J. Chem. Phys. **82**, 429 (1985).

[18] M. Pernice and H. F. Walker, SIAM J. Sci. Comput. **19**, 302 (1998).
[19] W. B. Streett and D. J. Tildesley, Proc. R. Soc. London, Ser. A **348**, 485 (1976).
[20] G. M. Torrie and G. N. Patey, Mol. Phys. **34**, 1623 (1977).
[21] F. G. Wang and D. P. Landau, Phys. Rev. E **64**, 056101 (2001).
[22] M. S. Shell, P. G. Debenedetti, and A. Z. Panagiotopoulos, Phys. Rev. E **66**, 056703 (2002).
[23] W. H. Press, B. P. Flannery, S. A. Teukolsky, and W. T. Vetterling, *Numerical Recipes in Fortran*, 2nd ed. (Cambridge University Press, Cambridge, UK, 1992).
[24] A. T. Gabriel, T. Meyer, and G. Germano, J. Chem. Theory Comput. (to be published), URL http://qmga.sourceforge.net.
[25] J. D. Parsons, Phys. Rev. A **19**, 1225 (1979).
[26] S.-D. Lee, J. Chem. Phys. **87**, 4972 (1987).
[27] S.-D. Lee, J. Chem. Phys. **89**, 7036 (1988).
[28] M. P. Allen, C. P. Mason, E. de Miguel, and J. Stelzer, Phys. Rev. E **52**, R25 (1995).
[29] D.-M. Duh and A. D. J. Haymet, J. Chem. Phys. **97**, 7716 (1992).
[30] A. Perera, G. N. Patey, and J. J. Weis, J. Chem. Phys. **89**, 6941 (1988).